Hardware Article

A low-cost and open-source measurement system to determine the Young's and shear moduli and Poisson's ratio of soft materials using a Raspberry Pi camera module and 3D printed parts

Matthew Sands, Jinki Kim *

Department of Mechanical Engineering, Georgia Southern University, P.O. Box 8046, Statesboro, GA 30460, USA

ABSTRACT

Advances in biomedical and engineering fields have greatly increased the need for understanding of soft structures. Soft materials such as gelatin and gelatin-based hydrogels have grown in popularity for use in a wide variety of applications including tissue engineering, biofabrication, and organ transplantation. With hydrogel structures being used in such demanding applications, it is crucial to properly characterize the dynamic behavior of these soft structures. Although there have been major improvements in measurement technology for determining the mechanical properties of soft, translucent materials, it remains quite challenging to reliably measure the Young's and shear moduli of these materials in a way that remains straightforward, low-cost, and non-contact. This research aims to address the weaknesses in modern measurement methods and develop a system suitable for characterizing the elastic moduli of soft materials that requires only four, inexpensive, off-the-shelf components. Utilizing a Raspberry Pi, stepping motor, and an inexpensive camera, the Young's and shear moduli of a gelatin column is measured five times. The standard deviation between measurement was observed to be less than 0.15% with high accuracy having an error of less than 4.6% when compared to relatively expensive, conventional measurement techniques.

© 2022 Published by Elsevier Ltd. This is an open access article under the CC BY-NC-ND license (http://creativecommons.org/licenses/by-nc-nd/4.0/).

Specifications table

Hardware name	Young's and shear moduli analyser for soft materials
Subject area	Engineering, biomedical and materials science
Hardware type	Measuring physical properties and in-lab sensors
Closest commercial analog	No commercial analog is available.
Open source license	GNU General Public License (GPL)
Cost of hardware	181 USD
Source file repository	https://doi.org/10.5281/zenodo.7116287

* Corresponding author.
 E-mail address: jinkikim@georgiasouthern.edu (J. Kim).

Hardware in context

Due to its unique material properties, gelatin and gelatin-based hydrogels are rapidly growing in popularity for use in a wide range of applications including tissue engineering [1] biofabrication [2], microfluidics [3,4], and soft robotics [5,6]. With soft structures often utilized in organ transplantation [2,7], tissue replacement [8], and 3D bioprinting [9], these gelatinous and soft structures are often subjected to dynamic motions as a result of an impact, vibrations, ultrasonic diagnostics, or excitation due to body movement in wearable electronics [1,10,11] and soft robotics [6]. Furthermore, since cell and tissue behavior are easily influenced by changes in the mechanical properties of their environment [12], the mechanical interaction between cells and their surrounding materials has become an area of interest for cancer and myocardial infarction research [13]. Therefore, determining the elastic properties of soft materials such as gelatin-based hydrogels is critical for understanding the dynamic behavior of the materials being employed in the aforementioned applications.

There have been various comprehensive research efforts to measure the Young's modulus [14,15] and shear modulus [16] of soft materials using both contact- and non-contact-based techniques. Static contact-based methods include techniques such as atomic force microscopy (AFM) indentation [17], tension/compression [18,19], and magnetic force-based methods [17], while dynamic testing is primarily performed via accelerometer or piezoelectric sensor [17,20]. Although conventional static contact-based measurement techniques provide reliable results for relatively stiff materials, these methods may be relatively slow and are not readily suitable for biofabrication or other fabrication processes. In addition, AFM indentation testing may be challenging for the measurement of hydrogels due to adhesion between the gelatin/hydrogel structure and the indentation punch [21]. Furthermore, dynamic contact-based measurement approaches may have large variable error due to the innate mass present from sensor contact [22,23].

Non-contact based dynamic measurement approaches such as laser, X-ray and magnetic resonance imaging (MRI) may also be used to characterize the mechanical properties of soft structures without mass loading effect [22,24]. However, lasers may produce inaccuracies due to reflection and absorption, especially with hydrogels that are typically translucent. As a result, reflective markers are often required for these approaches, which may provide substantial mass loading effect considering the pliable nature of soft matters in this study [25]. In addition, laser-based methods often have a limitation of measurement to a single point [25], making it challenging to obtain an object's mode shape without prior knowledge on the structure's material properties [26]. As a result, it is not readily available to identify the Young's and shear moduli simultaneously. Although scanning laser vibrometers can measure more than a single point, they are generally highly expensive, incapable of measuring low frequencies or large displacements, and cannot measure the response of an object sequentially [27]. X-ray and spectroscopy methods can be used to view the microstructure and nanostructure of hydrogels to evaluate the structural integrity of the sample, however these methods may lack the ability to characterize the material properties [24]. MRI-based methods often require expensive equipment compared to other conventional non-contact measurement approaches. Digital image correlation offers a relatively inexpensive, non-contact method for estimating the material properties of soft structures, but often requires a speckle pattern to be formed on the target structure's surface [30] and may even require multiple cameras [28,29]. On the other hand, optical flow method employed in the proposed study may be used to estimate the material properties of soft, translucent structures without the need for surface preparation or multiple cameras.

To advance the state of the art, this study presents a simple, open source, and cost-effective device to simultaneously determine the Young's and shear moduli of soft and translucent hydrogels using phase-based optical flow method, overcoming the drawbacks associated with laser-based commercial counterparts. The description of the hardware and its working principle with build and operation instructions are provided in the following sections. The reliability and accuracy of the proposed non-contact method are experimentally assessed by comparing its measurement results to those of conventional methods.

Hardware description

Despite modern advances in measurment technology, it is significantly challenging to reliably measure the elastic properties of translucent and soft materials using non-contact methods with a low-cost and straightforward implementation. The video-based method and the device proposed in this study enables the measurement of the elastic properties of soft materials in a non-contact and non-destructive manner.

The device is comprised of a stepping motor, a Raspberry Pi, and an affordable video camera, which builds up to a size for desktop use. A 3D printed arm attached to the motor provides an impulsive excitation to the soft material sample to induce a free vibration, which is recorded as a video. The video is then processed by the software package provided in this study to analyse the motion of the sample using phase-based motion estimation algorithm [27] that relates the phase shift of the pixel intensity to the displacement of the target structure captured in the video. A fast-Fourier transform is then performed on the resulting displacement signal to identify the resonant frequencies. Since the Young's and shear moduli primarily controls the flexural and torsional motions of the soft material, respectively, the material properties may be estimated when the corresponding resonant frequencies are known. However, without any prior knowledge of the material properties, it is challenging to identify which frequency peaks correspond to the flexural or torsional modes. On the other hand, since the optical flow in every pixel of the series of images captured by video effectively represents the motion of the target structure, the operational deflection shapes (effectively the mode shapes) can be assessed by utilizing phase-based motion magnification.

To do so, the phase signals from the image sequence are decomposed from the original video by using a set of complex steerable pyramid filters. The local phase signals are then temporally bandpassed near the resonance frequency and multiplied by amplification factor to magnify the motion of interest, the vibration mode shapes.

With the resonant frequencies and their corresponding mode shapes identified, the material properties may be obtained by utilizing the threoretical relationship between the Young's and shear moduli and the resonance frequencies. In this study, the soft material samples were prepared in vertical column shape with length L and width h, which could be modeled as cantilever beam based on Euler-Bernoulli beam theory. The fundamental natural frequency of flexural vibrations (ω_F) of a cantilever beam considering self-weight can be estimated as $\omega_F^2 = \omega_b^2 - \omega_g^2$ employing a single mode approximation [31]. Considering that gravity induced compression loading lowers the natural frequency of soft materials [32], $\omega_b = 3.516\sqrt{EI/\rho AL^4}$ and $\omega_g = 1.203\sqrt{g/L}$ are assumed, which represent the fundamental resonant frequencies of a cantilever beam and hanging chain, respectively [33]. E, A, and I represent the Young's modulus, cross section area, and the second moment of inertia, respectively. The fundamental natural frequency of torsional vibrations (ω_T) can be obtained as $\omega_T = \pi/2L\sqrt{CG/\rho J}$ where $C \approx 0.141h^4$ is the torsional constant considering the square cross section of the column. G and $J = (1/6)h^4$ are the shear modulus and polar area moment of inertia of the cross section about the axis of torsion, respectively [33]. Eq. (1) and (2) can then be obtained to determine the Young's and shear moduli respectively from the fundamental flexural and torsional natural frequencies determined by the experiment.
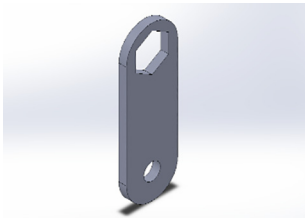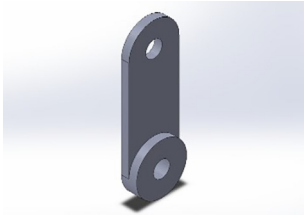
$$E = \left(\omega_F^2 + 1.203^2(g/L)\right)\left(\rho AL^4/3.516^2 I\right) \tag{1}$$

$$G = \rho J/C(2\omega_T L/\pi)^2 \tag{2}$$

The Poisson's ratio (v) may then be estimated based on the linear relationship between Young's and shear moduli assuming linear elastic isotropic behavior, $G = \frac{E}{2(1+v)}$. While gelatin at concentrations greater than 3% w/w have been shown to illustrate viscoelastic behavior, at low temperatures, over short time intervals, and low shear strain, gelatin is dominated by its elastic component under relatively small strain [34]. It is worth noting that the elastic properties of the soft material could be obtained as long as the sample is prepared into a shape in which the theoretical formula that relates the resonance frequency with the elastic moduli could be determined, like the column type presented above. Overall, the proposed device and software package for video-based measurement advances the state of the art by compiling a novel system that:
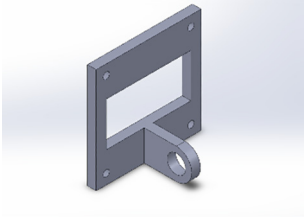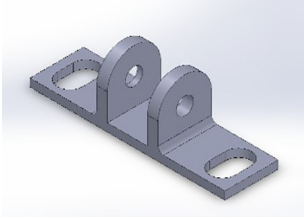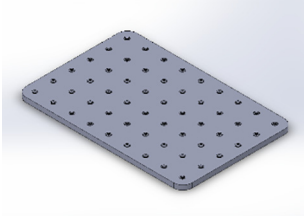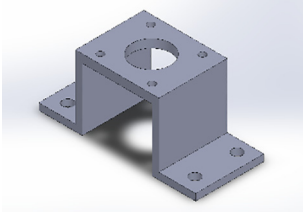
- Is capable of reliably and simultaneously measuring Young's and shear moduli of soft materials without inducing mass loading or requiring prior knowledge on the target structure.
- Has a minimal footprint allowing for maximum benchtop space.
- All parts may be printed with entry-level 3D printers requiring only four, inexpensive, off-the-shelf components (webcam module, motor, driver, and Raspberry Pi).

Design files summary
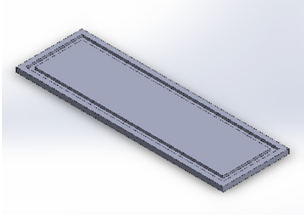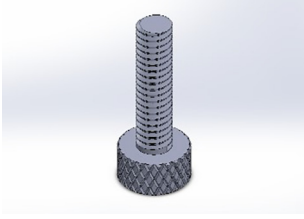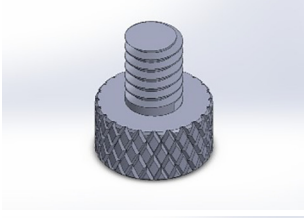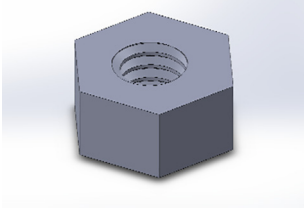
Part no.	Count	Design file name	Picture	File type	Open source license	Location of the file
A1	1	40mm_link_a		STEP-File (.STEP)	GPL	Zenodo Repository
A2	1	40mm_link_b		STEP-File (.STEP)	GPL	Zenodo Repository

(*continued*)

Part no.	Count	Design file name	Picture	File type	Open source license	Location of the file
A3	1	70mm_link_a		STEP-File (.STEP)	GPL	Zenodo Repository
A4	1	70mm_link_b		STEP-File (.STEP)	GPL	Zenodo Repository
A5	1	camera_adapter		STEP-File (.STEP)	GPL	Zenodo Repository
A6	1	table_adapter		STEP-File (.STEP)	GPL	Zenodo Repository
B1	1	base_plate		STEP-File (.STEP)	GPL	Zenodo Repository
C1	1	motor_mount		STEP-File (.STEP)	GPL	Zenodo Repository

(*continued*)

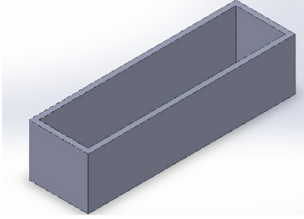| Part no.	Count	Design file name	Picture	File type	Open source license	Location of the file
C2	1	excitation_arm		STEP-File (.STEP)	GPL	Zenodo Repository
D1	1	mold_base		STEP-File (.STEP)	GPL	Zenodo Repository
D2	1	mold_shell		STEP-File (.STEP)	GPL	Zenodo Repository
E1	3	bolt_long		STEP-File (.STEP)	GPL	Zenodo Repository
E2	4	bolt_short		STEP-File (.STEP)	GPL	Zenodo Repository
E3	3	nut		STEP-File (.STEP)	GPL	Zenodo Repository
F1	1	prep_experiment	–	Python-File (.py)	GPL	Zenodo Repository
F2	1	run_experiment	–	Python-File (.py)	GPL	Zenodo Repository
F3	1	video_process	–	Compressed-Folder (.zip)	MIT	Zenodo Repository

Camera stand components (A1-6):

- 40mm_link_a is a 40 mm in length arm that makes up one link of the camera stand.
- 40mm_link_b is the second part of "link_a". This allows the stand to be printed with fewer supports.
- 70mm_link_a is similar to 40mm_link_a but 30 mm longer.
- 70mm_link_b is similar to 40mm_link_b but 30 mm longer.
- camera_adapter is the intermediate link between the 40 mm links and the Raspberry Pi camera. This allows the camera stand to hold the camera.
- table_adapter allows the 70 mm links to be mounted to the base plate. This completes the camera stand.

    System hardware (B1, E1-3):

- base_plate is the foundation for each system component to mount to and allow for a concise desktop system.
- bolt_long is a 25 mm thumb screw utilized to hold the camera stand together while also allowing for easy tension adjustment.
- bolt_short is a 8.7 mm thumb screw utilized to mount system components to the base plate.
- nut is the fastener utilized for both bolt variations.

    Excitation components (C1,2):

- motor_mount allows the stepping motor to be mounted to the base plate, keeping the motor in a consistent location.
- excitation_arm is the arm attached to the stepping motor which swipes the gelatin column to induce motion.

    Mold components (D1,2):

- mold_base is one of two parts for the mold. This is the bottom part that snaps on to the mold_shell.
- mold_shell is the wall portion of the mold. This part snaps on to the mold_base to complete the mold.

    Code library for material property extraction (F1-3):

- prep_experiment.py is the python code to preview the camera angle. This allows the camera to be adjusted to proper orientation prior to executing an experiment.
- run_experiment.py is the python code that executes an experiment. This records a video as the motor swipes the gelatin sample.
- video_process is a library of the video processing code which obtains the material properties from experimental data. The phase-based motion estimation algorithm that determines the displacement of the object is built upon the code published by Wadhwa et al. in [35].

Bill of materials summary

Designator	Component	Number	Cost per unit	Total cost	Source of materials	Material type
Raspberry Pi	Raspberry Pi Computer Model B	1	$ 117	$ 117	Amazon	Other
Raspberry Pi Camera	Arducam for Raspberry Pi Camera Module with Case	1	$ 22	$ 22	Amazon	Other
Stepper Motor	Usongshine Nema 17 Stepping Motor	1	$ 7	$ 7	Amazon	Metal
TB6600 Stepper Motor Driver	Usongshine Stepper Motor Driver TB6600	1	$ 10	$ 10	Amazon	Metal
Raspberry Pi Power Supply	CanaKit 5 V 2.5A Raspberry Pi 4 Power Supply	1	$ 10	$ 10	Amazon	Other
Stepper Motor Power Supply	EMITEVER 24 VDC Power Supply	1	$ 15	$ 15	Amazon	Other

- Raspberry Pi is the controller for both the camera and motor.
- Raspberry Pi Camera is the sensor utilized to measure displacement of the sample.

- Stepper motor automates the rotation of the excitation arm and allows for consistent excitation. However, since the excitation is a swiping motion that does not require any precise movement, the step resolution of the motor does not affect the excitation or measurement accuracy. A DC motor may be substituted if desired.
- TB6600 Stepper Motor Driver controls the stepper motor.

Build instructions

Module assembly

This section outlines the build instructions of the module to simultaneously measure the Young's and shear moduli using video-based vibrometry. After obtaining the required parts in the bill of materials, begin by 3D printing each component listed in the design files summary. The required quantity of each part is listed under the "count" column. Each part is recommended to be printed with 0.3 mm layer height, 20% infill, and supports, except for: "bolt_short", "bolt_long", and "nut". The nuts and bolts are recommended to be printed with 0.2 mm layer height with 100% infill and no supports considering the stress that may be applied when used in assembly. A typical polylactic acid (PLA) filament with 1.75 mm diameter is used for manufacturing the parts in this study using a Prusa MK3S + 3D printer. After printing, the camera stand may be assembled as follows (see Fig. 1):

- Bolt "70mm_link_a" (A3), "70mm_link_b" (A4), and "table_adapter" (A6) parts together. Reference the design files summary for part numbers.
- The 40 mm links (A1,2) may then be bolted to the 70 mm links.
- The "camera_adapter" (A5) may then be bolted to the 40 mm links.
- Lastly, the Raspberry Pi camera may be mounted to the stand as illustrated in Fig. 2(a).

Next, each component may be mounted to the "base_plate" (B1) as follows (see Fig. 2):

- Utilizing "stepper_mount" (C1) and "bolt_long" (E1), the stepper motor may be mounted to the "base_plate" (B1).
- The camera stand may then be mounted to the base plate. When using a specimen that has a size of 101.6 mm × 25.4 mm × 25.4 mm as utilized for verification in this study, the recommended mount point is as illustrated in Fig. 2.
- The "excitation_arm" (C2) may then be press fit on to the stepper motor and the camera mounted as shown in Fig. 2(b). The camera may be mounted via the nuts and bolts provided with the Raspberry Pi camera.
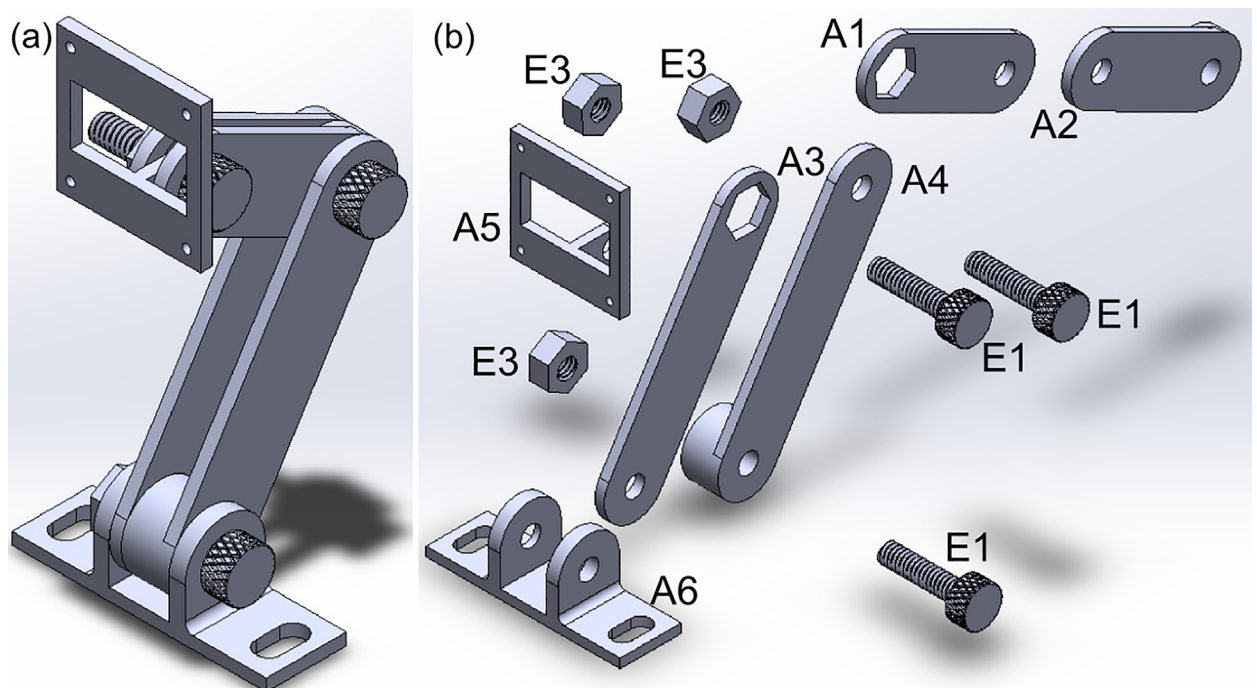
Fig. 1. Camera stand completed view (a) and exploded view (b). Part numbers in the Design file summary table are provided next to each component in the figure.
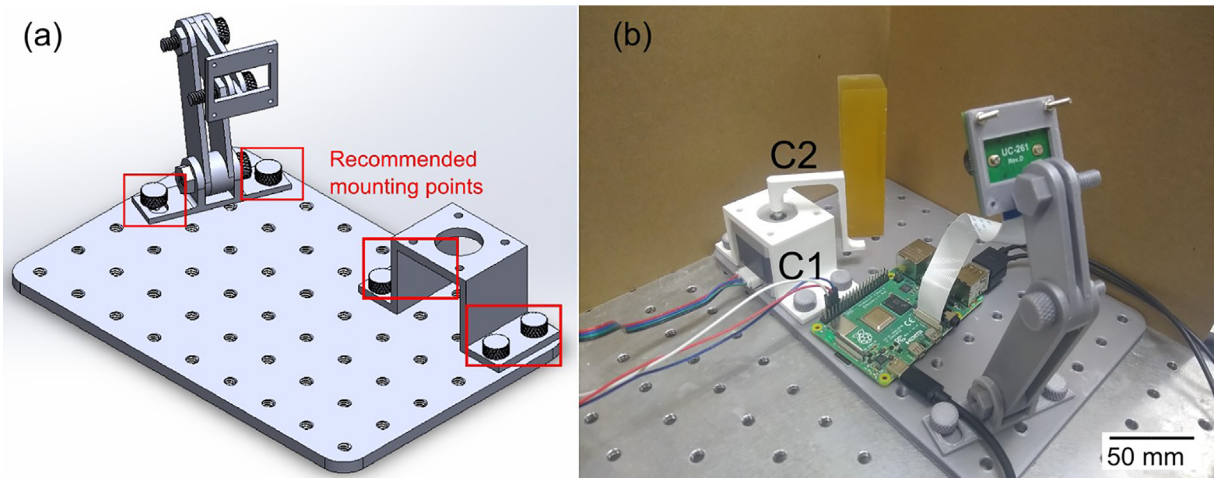
Fig. 2. Base plate completed view (a) and prepared for experiment (b). Part numbers in the Design file summary table are provided next to each component in the figure.

- The gelatin sample should be placed such that the "excitation arm" (C2) may swipe the edge of the sample inducing a small radial impulse. In this study, the excitation arm is allowed to strike the gelatin column with a depth of 1 mm; however, this value may require some adjustment depending on the stiffness of the structure being measured. Example videos are provided in "video_process" folder found in the Zenodo repository to illustrate the magnitude of excitation provided to the gelatin column. The gelatin is modeled as fixed-free, vertical, cantilever beam due to the inherent high adhesion between the specimen and the resting surface. No additional fixture or adhesive is required to fix the sample to the base plate.

Next the circuit may be wired together by connecting the stepping motor, motor driver, Raspberry Pi, and Raspberry Pi camera as illustrated in Fig. 3.

Preparing soft material samples

In this study, porcine gelatin (Sigma Aldrich, Catalog # G2625 with a Bloom number of 175 g according to the manufacturer) is utilized as a sample soft material to illustrate the effectiveness of the proposed approach, since gelatin is one of the
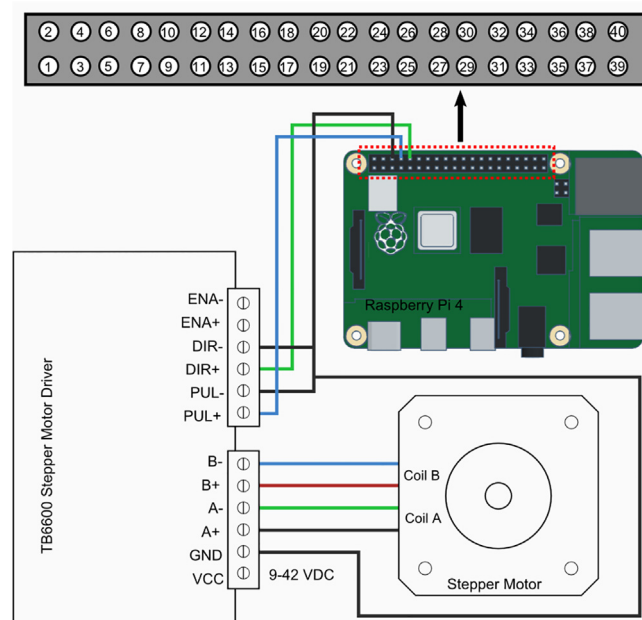
Fig. 3. Wiring diagram for the electronics of the video-based vibration measurement system.
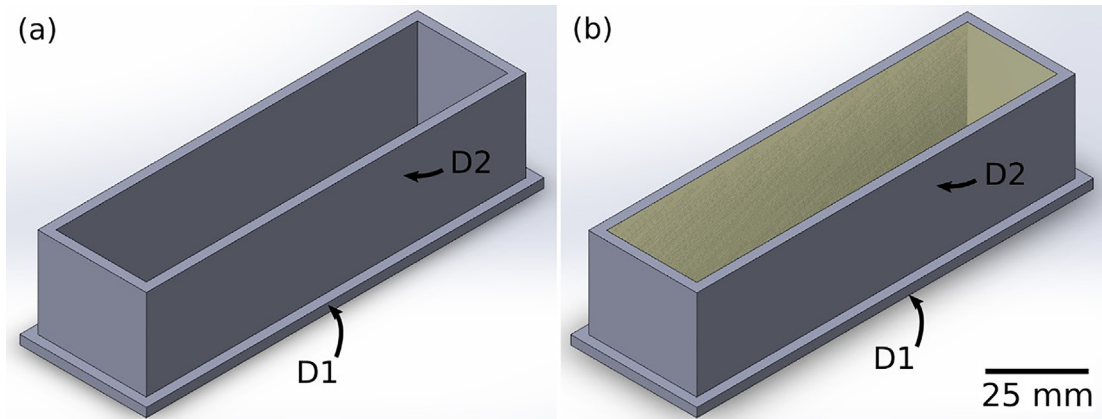
Fig. 4. Assembled (a) and filled (b) gelatin molds.

readily accessible soft and translucent materials that are often utilized in various applications. An easy-to-build gelatin specimen (25.4 mm × 25.4 mm × 101.6 mm) is prepared by utilizing a 3D printed mold provided in the design files summary. Note that the proposed method is greatly scalable based on appropriate setting of the camera and lens since the approach analyzes the motion of the object within the camera angle. Therefore, as long as the specimen is prepared into a shape in which theoretical formula for the resonance frequency can be obtained, like the column type presented in this study, the elastic properties of the material can be determined even with a different size specimen. The gelatin sample in this study is manufactured as follows (see Fig. 4):

- Determine a suitable gelatin concentration for your application and prepare the appropriate water and gelatin powder ratio. In this study, 25% w/w gelatin is utilized (75 g of water and 25 g of gelatin powder) for demonstration.
- Next, begin heating water to approximately 60 °C (140 °F). As the water heats, the sample mold (part D1 and D2 in the design file summary) may be prepared. The gelatin mold may be snapped together as illustrated in Fig. 4(a) and lubricated with a thin layer of oil. In this study, an olive oil-based cooking oil is utilized.
- Once the water reaches the desired 60 °C temperature, pour the gelatin powder in, and mix until homogenous, which took approximately 15 mins for 25% w/w concentration. It is recommended to mix thoroughly but quickly to reduce water evaporation.
- Next, pour the gelatin solution into the sample mold and refrigerate at approximately 10 °C (50 °F) for 1.5 h.
- After the sample has cured, it may be removed from the mold by popping the bottom off and gently pushing the gelatin sample out. It is recommended to allow the gelatin to return to room temperature prior to measurement.

Operation instructions

Hardware instructions

- Apply power to both the Raspberry Pi (5 V/2.5A) as well as the stepping motor driver (24 V/1.5A). This may be done via the "Raspberry Pi Power Supply" and "Stepper Motor Power Supply" listed in the bill of materials or by variable power supply.
- Place a gelatin sample on the "base_plate" (B1) such that the "excitation_arm" (C2) can swipe the edge of the sample while the camera records the response from an isometric view of the gelatin. The "excitation_arm" was allowed to strike the gelatin sample with a depth of 1 mm in this study as illustrated in Fig. 2(b); however, this value may require adjustment depending on size and stiffness of a given sample. An example video is provided with the "video_process" (F3) code package under the "data" directory. No additional constant intensity lighting or coatings are used in this study.

Software instructions

To prepare the camera for an experiment:

- The Raspberry Pi controls both the camera and the stepping motor and may be accessed directly by plugging in a mouse/keyboard to the USB-A ports and a display via HDMI port. Power the Pi by connecting the CanaKit 5 V Power Supply via the USB-C port labelled "power in". Once power is supplied, the Pi will boot into Raspberry Pi OS and prompt the user for initial setup (language, username, password, etc.). Afterwards, the user may login and continue to the next step in camera preparation.

- To ensure the camera is positioned as intended, execute "prep_experiment.py" (F1) which will display a preview of the camera's view. "prep_experiment.py" may be executed by running the command "python prep_experiment.py" in a terminal emulator.
- Adjust the position of the camera by loosening/tightening the bolts connecting the links together. Reference Fig. 5 for a frame image of the video illustrating the suggested field of view of the camera for adequately capturing the overall vibration patterns of the sample.

  To execute the experiment:

- The Raspberry Pi controls both the camera and the stepping motor.
- Executing "run_experiment.py" will begin video recording, spin the stepping motor to excite the structure via the excitation arm, and stop recording. "run_experiment.py" (F2) may be executed by running the command "python run_experiment.py" in a terminal emulator.
- To adjust any variable (i.e., recording time or motor speed), edit the "run_experiment.py" in any text editor or integrated development environment and adjust any variables listed at the top. Each variable and its use case are detailed in the code's comments.
  - "x_resolution" and "y_resolution" control the resolution in the horizontal and vertical directions, respectively.
    - It is worth noting that the resolution of the camera impacts the accuracy of the measurement. Since each pixel in the image sequence effectively serves as its own sensor, the greater the pixel density, the more precise the measurement. If the scale factor is too low, small motion may not be perceived since the motion is smaller than a single pixel. The scale factor in this study is approximately 8.54 pixels/mm.

  - "fs" is the framerate of the video (60 frames per second for this study).
    - The sampling rate or shutter speed of the camera is equally important as the resolution. According to Nyquist's theorem, the sampling rate of the sensor must be at least two times the frequency of the target structure's motion. For example, since the sampling rate is set to 60 Hz in this study, the maximum frequency that may be measured is 30 Hz. The sampling rate may need to be adjusted depending on the resonance frequencies of the sample.

  - "pulse_time" controls the speed of the motor via pulse width modulation. Decreasing "pulse_time" increases the motor speed and increasing "pulse_time" reduces the motor speed.
  - "record_time" is the length of time, in seconds, that the camera captures video. "record_time" should be long enough to capture the motion starting from excitation to when motion dies out. Eight seconds was chosen for this study.


Fig. 5. An example camera field of view that was used in this study for capturing the overall motion of the sample.

- After obtaining the video recording, the raw encoded video must be converted to MP4 format in order to be processed. This may be done by executing the following command in a terminal emulator: ffmpeg -framerate 30 -i /path/to/ video.h264 -c copy /path/to/video.mp4
  - It is worth noting that compressing the raw image data may introduce compression artifacts; however, it has been shown compressed video still offers excellent measurement accuracy even when compared to highly sensitive laser-based sensors [35–39]. Additionally, compression allows for faster processing times and limits the use of precious storage space.

To process the experimentally obtained data:

- The video processing code may be found in the compressed folder "video_process.zip" (F3). Download and extract this folder to obtain all the required code for the following steps.
- Open "trim_data.m" in MATLAB. This code is utilized to trim the length of videos such that only frames encompassing free vibration responses may be observed. This is achieved by allowing the user to select the time in which free vibration begins and the length of time that the measured structure oscillates. Executing the code will open a file manager which may then be used to select the experimental data one would like to process. The script will then load the videos and prompt the user for the length of time (in seconds) that the measured structure oscillates for. Typing the time and pressing enter will allow the script to proceed. Next, the script will prompt the user for the time (in seconds) that free vibration begins. Typing the time and pressing enter will trim the video and save it to the directory containing the original data under a folder titled "trimmed_data".
  - The process of selecting the initial time in which free vibration begins is made easier by displaying frame images from the video and their corresponding time stamp when executing the code. An example is shown in Fig. 6. By default, the code displays every 2nd frame between the time 1.5 s and 3 s. These parameters may be altered by adjusting the variables within the code. "time1" corresponds to the initial time (in seconds) frame images begin being displayed. "time2" corresponds to the time (in seconds) frame images cease to be displayed. "n_frames" corresponds to the nth frame to be displayed between the variables "time1" and "time2". For the video obtained in this study (included in "video_process.zip", F3), the excitation arm leaves the camera's field of view at approximately 2.43 s and the structure oscillates for 16 s so 2.43 is chosen as the initial trim time and 16 is chosen as the period of oscillation.
- Once the data has been trimmed, open "run_fft.m" in MATLAB. This code is utilized to obtain the frequency response of the target structure. Executing the code will open a file manager which may then be used to select the experimental data that one would like to process (the cropped videos). The script will then load the videos, carry out a fast-Fourier transform, display the frequency spectrum, and save it to the "cropped_data" directory under a folder titled "FFT".
  - The variable "fs" under "input settings" is the frame rate of the video being processed and should be set prior to executing the code. In this study, the videos are recorded at 60 frames per second (fps) so "fs" is taken as 60.
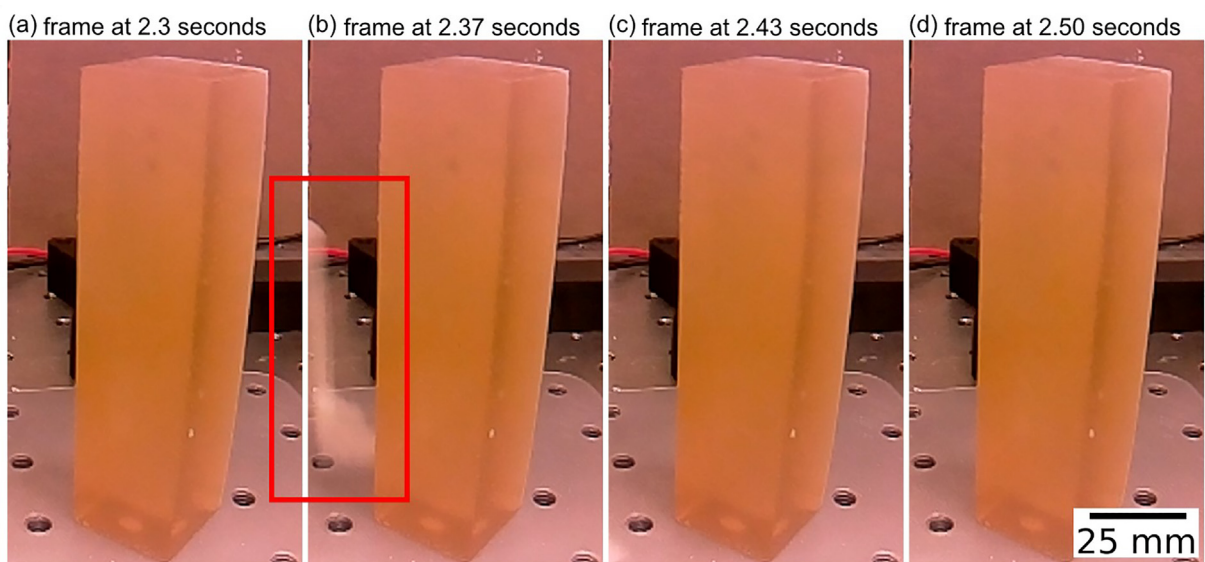
Fig. 6. Frame images from video of the gelatin sample being excited. Frame b illustrates the excitation arm (highlighted in red) swiping the structure at approximately 2.37 s. (For interpretation of the references to colour in this figure legend, the reader is referred to the web version of this article.)

- After obtaining the frequency response, the flexural and torsional resonant frequencies may be obtained. Open "evaluate_frequencies.m" in MATLAB. Executing the code will open a file manager which may then be used to select the experimental data that one would like to process (the cropped videos). The script will then load the videos and prompt the user for input frequencies. These should be the resonant frequencies identified from the spectrum previously obtained. The script will then prompt for the width of the frequency peak. This is the width of the peak obtained via the frequency spectrum. The script will then prompt the user for a magnification factor. This is the multiplication factor that the video will be amplified by. For soft structures with small displacements, a factor of 50 may be a safe starting point. The motions in the video will then be bandpass filtered around the frequencies of interest and magnified by the magnification factor provided by the user. The resulting videos will be saved to the "cropped_data" directory under a folder titled "magnification_results". The magnified videos should then be analyzed to determine which frequency corresponds to the respective flexural and torsional mode shapes.
- After identifying the frequencies corresponding to the flexural and torsional mode shapes, the material properties may be obtained. Open "evaluate_properties.m" in MATLAB. Executing the script will prompt the user to enter the flexural and torsional resonant frequencies. Afterwards, the script will calculate the Young's and shear moduli. The results will be displayed in the command window.
  - The mass, width, height, and length of the sample used for calculation may be adjusted by changing the "m", "w", "h", and "L" variables within the code, respectively.

Validation and characterization

Fig. 2(b) illustrates the completed test bench utilized to validate the effectiveness of the Raspberry Pi camera for measuring elastic and shear properties of soft hydrogels. In this case study for verification, a 25% w/w gelatin column was prepared as detailed in the operation procedure (*Sec.* 5.2). The experiment was performed to obtain five videos (720p resolution at 60 fps) of the column's free vibration response. The vibration of the gelatin sample was simultaenously measured by a laser displacement sensor (optoNCDT 1420, Micro-Epsilon) at a sampling rate of 4000 Hz with a reflector tape attached. The videos of the vibrating structures are then trimmed so that only frames encompassing the gleatin's free motion may be observed. The trimmed video is then processed to analyze the motion of the gelatin structure using phase-based motion estimation algorithm [35,37,39] and obtain the spectral response of the gelatin sample. The amplification factor is selected as 100 for this study to estimate the mode shapes of the samples. Capture images of the motion magnified videos are provided in Fig. 7(b,c) where the operational deflection shapes match the expected flexural and torsional mode shapes of the vertical cantilever beam.

In order to validate the repeatability of the proposed system, the fundamental resonant frequencies for the flexural and torsional vibration modes of a single 25% w/w gelatin sample were measured five times utilizing video. A Lorentzian fit is applied to the resulting frequency spectrum to obtain the resonant frequencies documented in Table 1, where the maximum
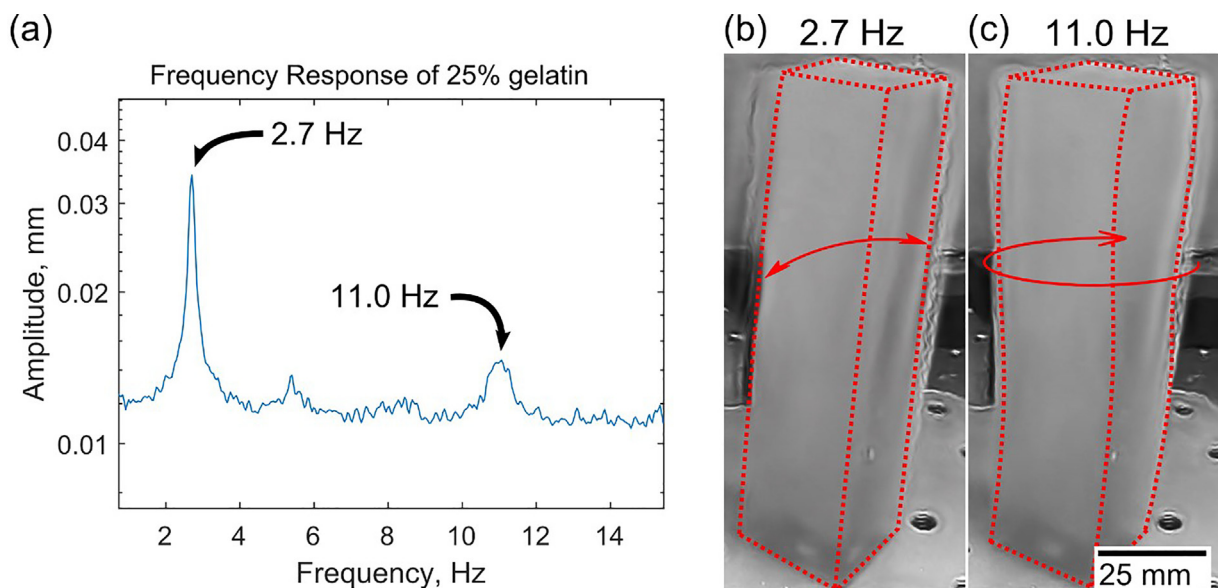

Fig. 7. Frequency response of a 25% gelatin sample (a) magnified at the highlighted resonant frequencies to obtain the flexural (b) and torsional (c) operational deflection shapes.

Table 1

Comparison of resonant frequencies from five video measurements of a single 25% w/w gelatin column.

	trial 1	trial 2	trial 3	trial 4	trial 5	mean	std. dev.	std. dev. %
Flexural resonance frequency, Hz	2.697	2.697	2.700	2.702	2.699	2.699	0.002	0.086
Torsional resonance frequency, Hz	10.992	11.027	10.995	11.009	10.998	11.004	0.014	0.131

standard deviation is less than 0.1% and 0.15%, respectively. These results support that the experimental setup provides reliable measurement of the vibration characteristic of the gelatin sample.

To verify the effectiveness of the proposed system, the time-series and resonance frequencies obtained by the Rasberry Pi camera-based method are compared to those simultaneously obtained by conventional laser displacement sensor utilzing the same 25% w/w gelatin sample used in consistency verfiication. The camera's sampling rate is maintained at 60 Hz and the laser displacement sensor is set to sample at 4 kHz. Both the laser and video signals are filtered using a Tukey window with a cosine/constant section ratio of 0.1 for leakage protection. The displacement from the camera was extracted using the local phase of the measured video as described in *Sec*. 2. To directly compare the time series results, the laser and video displacement signals were manually synced such that both measurements begin at the same time. The displacement derived from the camera closely matches the laser displacement signal with minimal amplitude and phase difference as illustrated in Fig. 8(a). Fig. 8(b) shows the frequency spectrum obtained by the two methods, which illustrate excellent agreement with a maximum difference of 1.1% when comparing the flexural resonant frequency and 3.3% when comparing the torisional resonant frequency, indicating that the video camera is calibrated with respect to the laser displacement sensor. Resonance frequencies and elastic moduli obtained by both approaches are provided in Table 2.

Following the experiments verifiying the consistency and accuracy of the proposed video-based approach, the reliability of the molding method is evaluated. Five gelatin samples were prepared for each of 20% w/w and 30% w/w gelatin concentrations as per the procedure detailed in *Sec*. 5.2. The time response of the gelatin samples are then measured by video camera and the elastic moduli are estimated. Table 3 provides the experimentally obtained mass densities, resonance frequencies, elastic moduli, and Poisson's ratios of each gelatin concentration. On average, the standard deviations of the Young's and shear moduli extracted from the proposed experiment respectively resulted in 3.2% and 3.5%, which supports that the experimental setup provides reliable measurement and fabrication of the gelatin structures.

The video based measurements were then compared with those of conventional compression techniques. The compression tests are performed on 5 samples for each of 20% and 30% gelatin concentrations utilizing a material testing system (ESM303, Mark-10 Corporation). The gelatin samples for each concentration are compressed by 7.5% of their overall length at three different compression rates: 0.21%/s, 0.41%/s, and 0.84%/s for a total of 30 measurements. A single stress–strain curve is presented in Fig. 9(a) where a linear fit is applied to the entire length of the curve and the slope of the fitted line is taken as the Young's modulus.The mean and standard deviation of the Young's moduli determined for each compression rate are provided in Table 4. The fitted results are illustrated in Fig. 9(b) where the thick bold lines indicate the average of five measurements for a given concentration and compression rate. It may be noted from Fig. 9(b) that varied compression rate has little impact on the stress–strain curve's linearity with a deviation of 1.1% between the average coeffecents of determination.
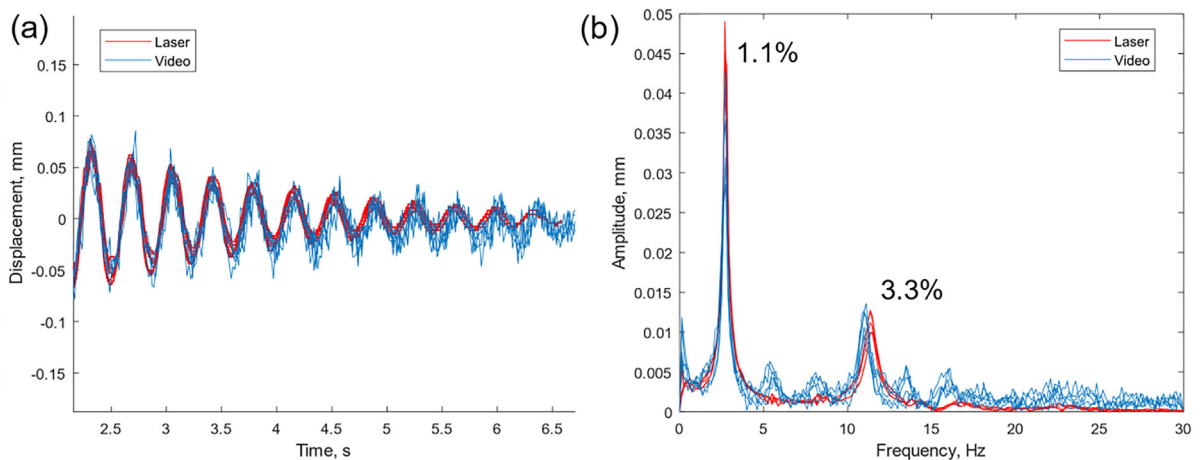
Fig. 8. Comparison of the time series (a) and frequency response (b) from five measurements of a single 25% w/w gelatin sample using laser and video techniques.

Table 2
Comparison of resonant frequencies and elastic moduli from five measurements of a single 25% w/w gelatin sample using laser and video techniques.

	Video	Laser	Difference, %
Flexural resonance frequency, Hz	2.70 ± 0.00	2.73 ± 0.01	1.1
Torsional resonance frequency, Hz	11.00 ± 0.01	11.38 ± 0.03	3.3
Young's modulus, kPa	71.0 ± 0.1	72.1 ± 0.1	1.5
Shear modulus, kPa	24.5 ± 0.1	26.2 ± 1.0	6.5

Table 3
Comparison of resonant frequencies and elastic moduli from five measurements of 20% w/w and 30% w/w gelatin samples using video techniques.

| Concentration	20%	30%
Density, kg/m3	1026.3 ± 15.1	1076.5 ± 27.5
Flexural resonance frequency, Hz	2.37 ± 0.09	4.57 ± 0.11
Torsional resonance frequency, Hz	9.88 ± 0.02	17.30 ± 0.10
Young's modulus, kPa	55.4 ± 1.8	162.7 ± 7.3
Shear modulus, kPa	18.8 ± 0.7	62.1 ± 2.0
Poisson's ratio	0.47 ± 0.04	0.31 ± 0.04
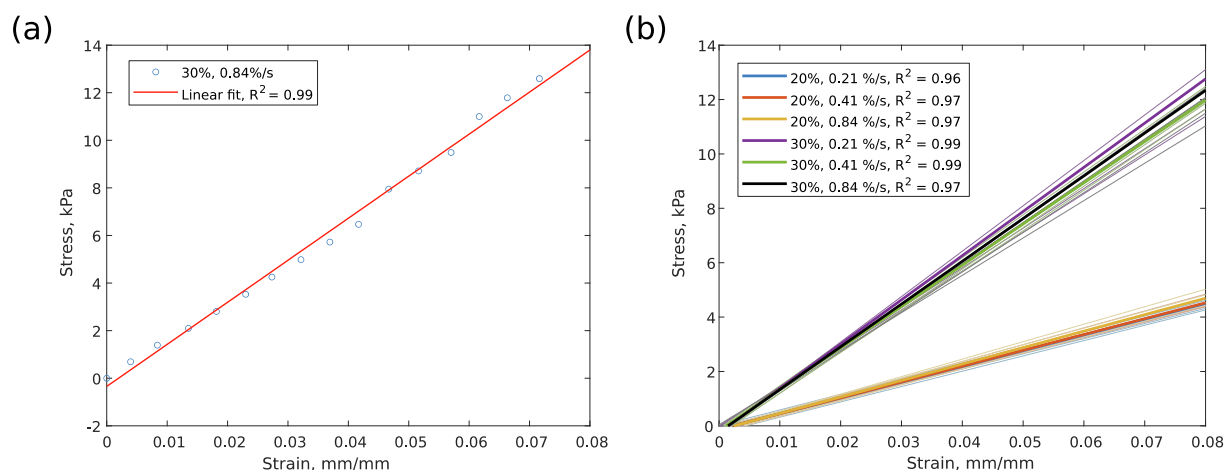
Fig. 9. (a) Stress–strain curve of a single gelatin column measurement and (b) linear fitted stress–strain curves for varied compression rates. Thick lines indicate average of individual measurements that are presented by light-colored lines.

Table 4
Comparison of Young's modulus obtained at varied compression rates for both 20% and 30% gelatin concentrations.

Concentration	20%	30%
Deformation rate, 0.21%/s	57.2 ± 1.3 kPa	151.7 ± 9.5 kPa
Deformation rate, 0.41%/s	58.1 ± 2.2 kPa	153.4 ± 3.8 kPa
Deformation rate, 0.84%/s	60.0 ± 2.8 kPa	150.8 ± 9.1 kPa

Comparing the video and compression results for both 20% w/w and 30% w/w concentrations show great quantitative agreement with minimal variation as illustrated in Fig. 10.

In summary, this research investigates a low-cost and open-source method that can simultaneously measure the Young's and shear moduli of soft structures, such as translucent hydrogels. The material properties are determined by measuring the resonance frequencies and mode shapes from a single video captured by a Raspberry Pi camera. Utilizing an analytical solution, the resonant frequencies may be related to the Young's and shear moduli without requiring any prior knowledge on the material properties of target structure or inducing contact-based mass loading, a critical point for measurement of soft structures. Thus, the proposed method yields a straightforward implementation that requires only a low-cost digital camera without the need of special equipment. Through experimental investigations on a gelatin-based hydrogel sample it is found that
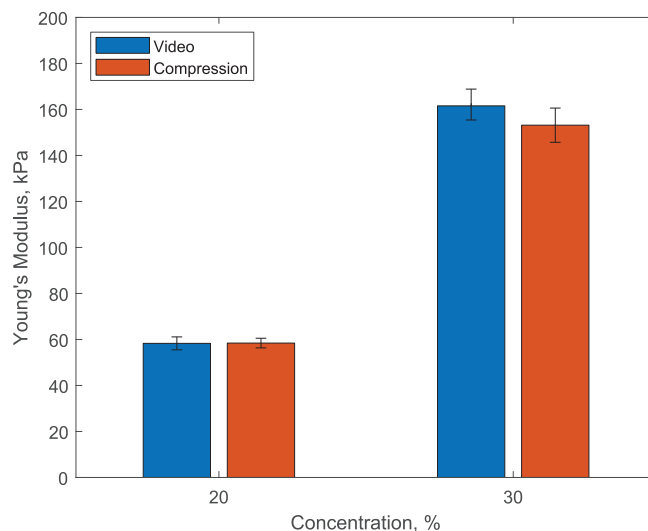
Fig. 10. Comparison of Young's modulus obtained by both video and compression techniques.

the proposed method reliably identifies the mechanical properties of the soft structure when compared to that with leading conventional measurement methods. The results of this study illustrate promising potential for implementing the proposed methodology in various fields such as cell biology and engineering applications including soft robotics, wearable sensors, tissue engineering and biofabrication.

Declaration of Competing Interest

The authors declare that they have no known competing financial interests or personal relationships that could have appeared to influence the work reported in this paper.

Acknowledgments

References

[1] J. Chen, Q. Peng, T. Thundat, H. Zeng, Stretchable, Injectable, and Self-Healing Conductive Hydrogel Enabled by Multiple Hydrogen Bonding toward Wearable Electronics, Chem. Mater. 31 (12) (2019) 4553–4563, https://doi.org/10.1021/acs.chemmater.9b01239.
[2] A.S. Munoz-Abraham, C. Ibarra, R. Agarwal, J. Geibel, D.C. Mulligan, 3D Bioprinting in Transplantation, in: S.N. Nadig, J.A. Wertheim (Eds.), Technological Advances in Organ Transplantation, Springer International Publishing AG, 2017, pp. 261–276, https://doi.org/10.1007/978-3-319-62142-5.
[3] M.P. Cuchiara, A.C.B. Allen, T.M. Chen, J.S. Miller, J.L. West, Multilayer microfluidic PEGDA hydrogels, Biomaterials 31 (21) (Jul. 2010) 5491–5497, https://doi.org/10.1016/j.biomaterials.2010.03.031.
[4] N. Annabi et al, Hydrogel-coated microfluidic channels for cardiomyocyte culture, Lab Chip 13 (18) (2013) 3569, https://doi.org/10.1039/c3lc50252j.
[5] M. Baumgartner et al, Resilient yet entirely degradable gelatin-based biogels for soft robots and electronics, Nat. Mater. 19 (10) (Oct. 2020) 1102–1109, https://doi.org/10.1038/s41563-020-0699-3.
[6] B. Ying, X. Liu, Skin-like hydrogel devices for wearable sensing, soft robotics and beyond, iScience 24 (11) (2021), https://doi.org/10.1016/j.isci.2021.103174 103174.
[7] M.M. Stanton, J. Samitier, S. Sánchez, Bioprinting of 3D hydrogels, Lab Chip 15 (15) (Aug. 2015) 3111–3115, https://doi.org/10.1039/c5lc90069g.
[8] S. Woerly, G.W. Plant, A.R. Harvey, Neural tissue engineering: from polymer to biohybrid organs, Biomaterials 17 (3) (Feb. 1996) 301–310, https://doi.org/10.1016/0142-9612(96)85568-2.
[9] Y.-Z. Yu, L.-L. Zheng, H.-P. Chen, W.-H. Chen, Q.-X. Hu, Fabrication of hierarchical polycaprolactone/gel scaffolds via combined 3D bioprinting and electrospinning for tissue engineering, Adv. Manuf. 2 (3) (Sep. 2014) 231–238, https://doi.org/10.1007/s40436-014-0081-2.
[10] F. He et al, Stretchable, Biocompatible, and Multifunctional Silk Fibroin-Based Hydrogels toward Wearable Strain/Pressure Sensors and Triboelectric Nanogenerators, ACS Appl. Mater. Interfaces 12 (5) (Feb. 2020) 6442–6450, https://doi.org/10.1021/acsami.9b19721.
[11] S. Zeng, J. Zhang, G. Zu, J. Huang, Transparent, flexible, and multifunctional starch-based double-network hydrogels as high-performance wearable electronics, Carbohydr. Polym. 267 (Sep. 2021), https://doi.org/10.1016/j.carbpol.2021.118198 118198.
[12] W. Gross, H. Kress, Simultaneous measurement of the Young's Modulus and the Poisson Ratio of thin elastic layers, Soft Matter 13 (2017), https://doi.org/10.1039/C6SM02470J.
[13] A.W. Holle et al, Cell–Extracellular Matrix Mechanobiology: Forceful Tools and Emerging Needs for Basic and Translational Research, Nano Lett. 18 (1) (Jan. 2018) 1–8, https://doi.org/10.1021/acs.nanolett.7b04982.
[14] G.-W. Kim, G.-S. Do, Y. Bae, Y. Sagara, Determination of the Viscoelastic Properties of Agar/Agar-Gelatin Gels Based on Finite Element Method Optimization, FSTR 14 (6) (2008) 525–532, https://doi.org/10.3136/fstr.14.525.

[15] Y. Wen, C. Xu, H. Wang, A. Chen, R.C. Batra, Impact of steel spheres on ballistic gelatin at moderate velocities, Int. J. Impact Eng 62 (Dec. 2013) 142–151, https://doi.org/10.1016/j.ijimpeng.2013.07.002.

[16] P. Bender, A. Tschöpe, R. Birringer, Determination of the shear modulus of gelatine hydrogels by magnetization measurements using dispersed nickel nanorods as mechanical probes, J. Magn. Magn. Mater. 346 (Nov. 2013) 152–160, https://doi.org/10.1016/j.jmmm.2013.07.010.

[17] D. Lee, H. Zhang, and S. Ryu, "Elastic Modulus Measurement of Hydrogels," 2018, pp. 1–21. doi: 10.1007/978-3-319-76573-0_60-1.

[18] A. Engler, L. Bacakova, C. Newman, A. Hategan, M. Griffin, D. Discher, Substrate compliance versus ligand density in cell on gel responses, Biophys. J . 86 (1 Pt 1) (Jan. 2004) 617–628, https://doi.org/10.1016/S0006-3495(04)74140-5.

[19] R. J. J. Pelham and Y. l Wang, "Cell locomotion and focal adhesions are regulated by substrate flexibility.," *Proc Natl Acad Sci U S A*, vol. 94, no. 25, pp. 13661–13665, Dec. 1997, doi: 10.1073/pnas.94.25.13661.

[20] A. Markidou, W. Shih, W.-H. Shih, Soft-materials elastic and shear moduli measurement using piezoelectric cantilevers, Rev. Sci. Instrum. – Rev. Sci. Instr. 76 (2005), https://doi.org/10.1063/1.1928407.

[21] M. Czerner, L.S. Fellay, M.P. Suárez, P.M. Frontini, L.A. Fasce, Determination of elastic modulus of gelatin gels by indentation experiments, Procedia Mater. Sci. 8 (2015) 287–296, https://doi.org/10.1016/j.mspro.2015.04.075.

[22] S. Schwarz et al, Contactless vibrational analysis of transparent hydrogel structures using laser-doppler vibrometry, Exp. Mech. 60 (2020), https://doi.org/10.1007/s11340-020-00626-0.

[23] A. Yadav, N.K. Singh, Investigation for accelerometer mass effects on natural frequency of magnesium alloy simply supported beam, Mater. Today:. Proc. 28 (2020) 2561–2565, https://doi.org/10.1016/j.matpr.2020.05.279.

[24] H.S. Mansur, R.L. Oréfice, A.A.P. Mansur, Characterization of poly(vinyl alcohol)/poly(ethylene glycol) hydrogels and PVA-derived hybrids by small-angle X-ray scattering and FTIR spectroscopy, Polymer 45 (21) (2004) 7193–7202, https://doi.org/10.1016/j.polymer.2004.08.036.

[25] K. Ohtani, L. Li, and M. Baba, "Determining surface shape of translucent objects by using laser rangefinder," in *Proceedings of the 2013 IEEE/SICE International Symposium on System Integration*, Kobe, Japan, 2013, pp. 454–459. doi: 10.1109/SII.2013.6776744.

[26] B. Wang, A.G. Moura, J. Chen, A. Erturk, Y. Hu, Characterization of hydrogel structural damping, Extreme Mech. Lett. 40 (2020), https://doi.org/10.1016/j.eml.2020.100841 100841.

[27] A. Sarrafi, Vibration-based damage detection in wind turbine blades using Phase-based Motion Estimation and motion magnification, J. Sound Vib. (2018) 19.

[28] W. He, Q. Duan, W. Shi, H. Xie, Elastic property characterization of soft substrate-supported thin films using multiscale digital image correlation, Opt. Lasers Eng. 121 (2019) 112–119, https://doi.org/10.1016/j.optlaseng.2019.03.003.

[29] T.-I. Lee, M.S. Kim, T.-S. Kim, Contact-free thermal expansion measurement of very soft elastomers using digital image correlation, Polym. Test. 51 (2016) 181–189, https://doi.org/10.1016/j.polymertesting.2016.03.014.

[30] Y. Yang et al, Blind identification of full-field vibration modes from video measurements with phase-based video motion magnification, Mech. Syst. Sig. Process. 85 (2017) 567–590, https://doi.org/10.1016/j.ymssp.2016.08.041.

[31] J. Kim, P. Dorin, K.W. Wang, Vibration energy harvesting enhancement exploiting magnetically coupled bistable and linear harvesters, Smart Mater. Struct. 29 (6) (Jun. 2020), https://doi.org/10.1088/1361-665X/ab809a 065006.

[32] L.N. Virgin, S.T. Santillan, D.B. Holland, Effect of gravity on the vibration of vertical cantilevers, Mech. Res. Commun. 34 (3) (2007) 312–317, https://doi.org/10.1016/j.mechrescom.2006.12.006.

[33] R. Blevins, Formulas for Dynamics, Acoustics and Vibration, John Wiley & Sons Ltd (2016).

[34] J. van Otterloo, A.R. Cruden, Rheology of pig skin gelatine: Defining the elastic domain and its thermal and mechanical properties for geological analogue experiment applications, Tectonophysics 683 (2016) 86–97, https://doi.org/10.1016/j.tecto.2016.06.019.

[35] N. Wadhwa, M. Rubinstein, F. Durand, W.T. Freeman, Phase-based video motion processing, ACM Trans. Graph. 32 (4) (Jul. 2013) 1–10, https://doi.org/10.1145/2461912.2461966.

[36] Y.-J. Cha, J.G. Chen, O. Büyüköztürk, Output-only computer vision based damage detection using phase-based optical flow and unscented Kalman filters, Eng. Struct. 132 (2017) 300–313, https://doi.org/10.1016/j.engstruct.2016.11.038.

[37] J.G. Chen, N. Wadhwa, Y.J. Cha, F. Durand, W.T. Freeman, O. Buyukozturk, Modal identification of simple structures with high-speed video using motion magnification, J. Sound Vib. 345 (2015) 58–71, https://doi.org/10.1016/j.jsv.2015.01.024.

[38] J.G. Chen, A. Davis, N. Wadhwa, F. Durand, W.T. Freeman, O. Büyüköztürk, Video camera-based vibration measurement for civil infrastructure applications, J. Infrastruct. Syst. 23 (3) (2017) B4016013, https://doi.org/10.1061/(ASCE)IS.1943-555X.0000348.

[39] P. Poozesh, A. Sarrafi, Z. Mao, P. Avitabile, C. Niezrecki, Feasibility of extracting operating shapes using phase-based motion magnification technique and stereo-photogrammetry, J. Sound Vib. 407 (2017) 350–366, https://doi.org/10.1016/j.jsv.2017.06.003.

Matthew Sands received his B.S. degree in mechanical engineering from Georgia Southern University, Statesboro in 2021. Currently, he pursing a M.Sc degree in mechanical engineering at Georgia Southern University. His current research interest is focused on structural health monitoring.

Jinki Kim is an Assistant Professor in the Department of Mechanical Engineering at Georgia Southern University, Statesboro, GA USA. Prior to joining Georgia Southern University, he received his Ph.D degree in mechanical engineering from the University of Michigan, MI USA. His current research interests include design, analysis, and implementation of electromechanical sensors and actuators, structural health monitoring, and advanced manufacturing.